ORIGINAL RESEARCH ARTICLE

Toroidal Dipole All-Dielectric Metasurfaces with High Sensitivity, High Figure of Merit, and Robustness for Refractive Index Sensing

Yanyan Zheng[1] · Ying Chen[1] · Yingying Xu[1]

Abstract

Refractive index sensing is of great significance in biological detection. Especially, all-dielectric metasurfaces can greatly improve the sensitivity of biological detection. However, the Q factor and electric field enhancement of most metasurfaces are generally low, resulting in low sensitivity and figure of merit (FOM). Meanwhile, fabrication tolerances may result in inability to achieve high-performance refractive index sensing. Here, we use finite element method (FEM) simulation to design a conical hole structure on an all-dielectric metasurface. The toroidal dipole resonance based on a conical hole structure can achieve a large-area electric field enhancement and a high Q factor, thereby achieving a sensitivity of 540 nm/RIU and FOM of 154.3. Meanwhile, considering the real fabrication tolerance, the proposed structure can still achieve high-sensitivity sensing when the conical hole structure changes the ellipsoidal structure. Therefore, the high sensitivity, high FOM, and robustness of the proposed structure make it highly significant for practical applications.

Keywords Metasurfaces · toroidal dipole · high sensitivity · robustness · refractive index sensing

Introduction

Due to the advantages of high sensitivity, high selectivity, low cost, and so on,[1–3] optical biosensors play an important role in modern biomedical, material, and environmental monitoring applications.

In recent years, metasurfaces[4–6] have emerged as a crucial area for advancing the development of optical sensing technology. Metasurfaces are optical devices composed of subwavelength structures that can be designed reasonably to achieve specific functions.[7–9] For optical sensing, metasurfaces can confine light to micro/nanoscale electromagnetic hotspots to improve sensitivity. In addition, due to the important role played by the anopole mode in regulating the light field,[10,11] the anopole metasurface can also be applied to optical sensing.[12] Metasurface optical sensors have been applied in many works.[13–16]

Refractive index sensors are one of the most common types of optical biosensors.[17–19] When the refractive index of the analyte increases, it will cause a redshift of resonance.

The sensitivity is defined as the ratio of the shift of the resonance peak to the change in refractive index.[20] In addition, the change in resonance intensity can also be used as a detection indicator for refractive index sensing.[21] However, the main problem currently limiting the performance of refractive index sensors is the weak interaction between the light field and the analyte, resulting in low sensitivity. At present, most methods enhance the interaction between light and analytes by increasing the Q factor, including the coupling of localized surface plasmon resonance with surface lattice modes, high-refractive-index dielectric materials, and Fano resonance structures.[22–24] Due to the near-field enhancement and strong nonlinear effects, toroidal dipole resonance also can significantly enhance the interaction between light and matter.[25,26] Therefore, Wang et al.[27] designed the toroidal dipole to achieve high sensitivity by using a strong electric field generated near the microstructure interface around the toroidal dipole. Moreover, as a new method for achieving an infinite Q factor, bound states in the continuum (BIC) have been proposed.[27–30] High-Q and high-sensitivity sensing can be achieved by quasi-BICs.[31–33] Although the BIC can achieve high Q factor and high figure of merit (FOM), most studies have found that electric field enhancement is localized in a small area, resulting in weak interaction between light and analytes, and the sensitivity is still not suboptimal.

✉ Yingying Xu
    yyxu@tzc.edu.cn

1   Department of Computer Science, Taizhou University,
    Zhejiang 318000, China

Plasma plays a crucial role in confining and manipulating local electromagnetic fields. However, in optical frequencies, metals exhibit significant losses, leading to a low Q factor. Moreover, fabrication tolerances can reduce the Q factor, which results in an inability to achieve high-performance refractive index sensing. Due to the low loss of dielectric material, all-dielectric metasurfaces with high Q can be achieved. Therefore, we have designed a conical hole structure for all-dielectric metasurfaces. The toroidal dipole resonance mode achieved by using the conical hole structure not only can achieve a high Q factor, but also can achieve large-area electric field enhancement, thus achieving high refractive index sensitivity sensing and high FOM. We also confirm the strong robustness of the structure.

Structure and Model

Figure 1 shows the designed all-dielectric conical hole unit structure. The side length L of the unit is 1 μm, height H is 0.2 μm, and the upper diameter D of the conical hole is 0.7 μm. The material is glass (LaSF), with a fixed refractive index of 1.8. Here, the finite element method (FEM) is
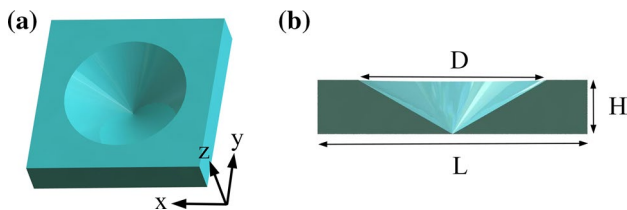

Fig. 1 (a) The three-dimensional unit structure of the metasurface; (b) cross-section of the unit structure.

used for simulation, with the electric field polarized in the X direction and the wave vector incident perpendicular to the metasurface in the Z direction. Periodic conditions are set in the X and Y directions, and the Z direction is defined as a perfectly matched layer. To avoid interference, the monitor is placed at a distance of 10 μm from the surface of the structure.

Results and Discussion

Firstly, the effect of the conical hole bottom radius on the transmission of the structure was studied. The circular hole can obtain two obvious resonances when the bottom radius is 0.35 μm, as indicated in Fig. 2a. As the bottom radius of the conical hole decreases to 0 μm, the resonance line width of long wavelengths is significantly reduced, while the change in short wavelength resonance is not very significant. The narrower the resonance peak, the higher the Q factor obtained. Therefore, the bottom radius of the conical hole chosen here is 0 μm for further research. As shown in Fig. 2b, the wavelengths of the two resonances are 1.087 μm and 1.255 μm, and the corresponding Q factors are 1767.4 and 173.7. Compared to the Q factor of resonance at 1.255 μm, the Q factor of resonance at 1.087 μm is about 10 times higher.

A higher Q factor does not necessarily lead to high refractive index sensitivity. Therefore, these two resonance modes need further research. To analyze the electromagnetic resonance modes of these two resonances, multipole decomposition can be performed by integrating the current density of the structure in the Cartesian coordinate system.[34,35] Multipole resonance can be written in the form of the following current description:
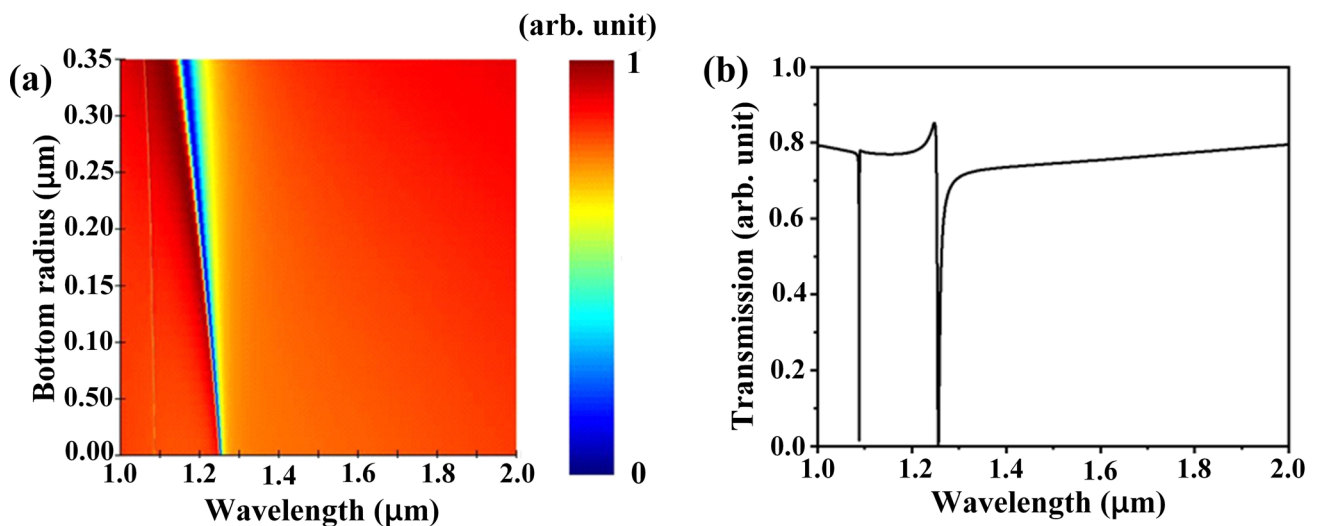

Fig. 2 (a) Transmission with varying bottom radius; (b) transmission of the bottom radius of 0 μm.

Electric dipole (ED):

$$P = -\frac{1}{iw} \int j d^3 r \tag{1}$$

Magnetic dipole (MD):

$$M = \frac{1}{2c} \int (r \times j) d^3 r \tag{2}$$

Toroidal dipole (TD):

$$T = \frac{1}{10c} \int \left[(r \cdot j)r - 2r^2 j \right] d^3 r \tag{3}$$

Electric quadrupole (EQ):

$$Q_{\alpha\beta} = -\frac{1}{2iw} \int \left[r_\alpha j_\beta + r_\beta j_\alpha - \frac{2}{3}(r \cdot j)\delta_{\alpha\beta} \right] d^3 r \tag{4}$$

Magnetic quadrupole (MQ):

$$M_{\alpha\beta} = \frac{1}{3c} \int \left[(r \times j)_\alpha r_\beta + (r \times j)_\beta r_\alpha \right] d^3 r \tag{5}$$

where j is the surface current density, c is the speed of light in vacuum, and r is the displacement vector. Only ED, MD, TD, EQ, and MQ have been calculated here, as shown in Fig. 3a. It can be observed that the resonance at 1.087 μm is mainly EQ and MD, while the resonance at 1.255 μm is mainly TD resonance. Meanwhile, the impedance of the metasurface can be calculated by the impedance formula. The formula is as follows:[36]

$$Z = \sqrt{\frac{(1 + S_{11})^2 - S_{21}^2}{(1 - S_{11})^2 - S_{21}^2}} \tag{6}$$

where S_{11} and S_{21} represent the reflection and transmission, respectively. As shown in Fig. 3b, the effective impedance of the two resonances is $Z = 0.02 + 1.09i$ and $Z = 0.00 + 0.79i$. Because the transmission of the two resonances approaches zero, the real part of the impedance is close to zero, and the imaginary part of the impedance is close to 1.[37]

Since it is different from traditional EDs and MDs, the TD can greatly promote the interaction between light and matter, and is extremely sensitive to environmental changes. Equations (7) and (8) are the electric field radiation of traditional dipole and toroidal dipole resonance, respectively.[38] From one of the equations, it can be seen that, compared to dipole resonance, the electric field of the TD is more sensitive to changes in environmental refractive index. By utilizing the characteristics of the TD, highly sensitive biosensing can be achieved. For refractive index sensing, the TD plays an important role, and future research needs to focus on TDs.

$$E_P = n^2 k_0^2 \left(\hat{r} \times \hat{r} \times \frac{\hat{P}}{r} \right) \tag{7}$$

$$E_T = n^3 k_0^3 \left(\hat{r} \times \hat{r} \times \frac{\hat{T}}{r} \right) \tag{8}$$

To further analyze the resonance modes, we analyzed the electromagnetic fields of these two resonances, as shown in Fig. 4. Figure 4a, c and b, d show the cross-section position at $Z = 0$ μm and $X = 0$ μm, respectively. Figure 4a shows the electric field at 1.255 μm. The black arrow indicates the current vector, and the blue arrow indicates the direction. The direction of the middle electric field and the upper and lower electric fields are opposite. The middle and upper electric fields can form an upward magnetic field, while the middle and lower magnetic fields can form a downward magnetic field, which is also proven by Fig. 4b. The
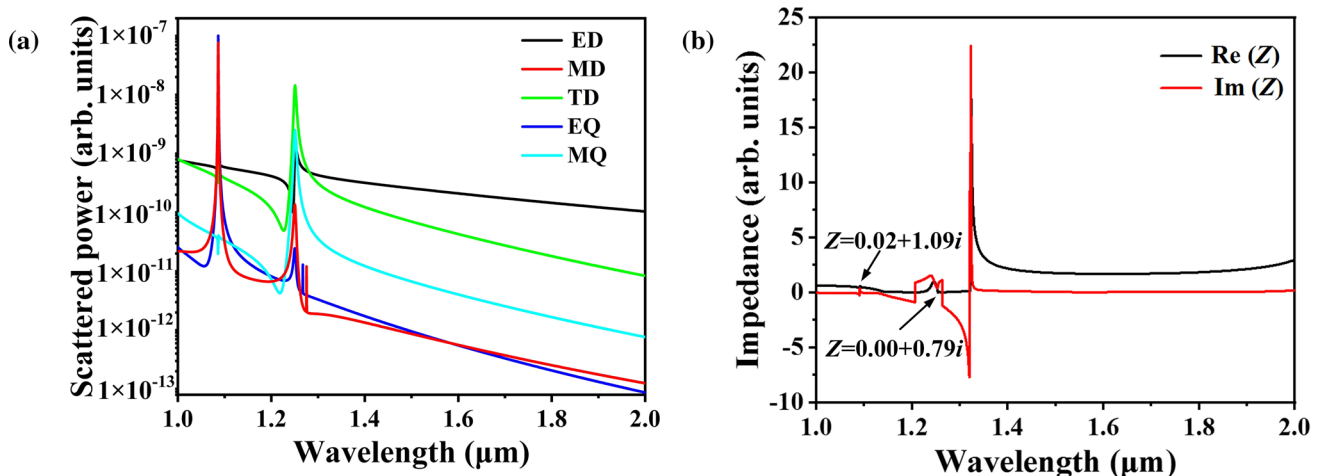

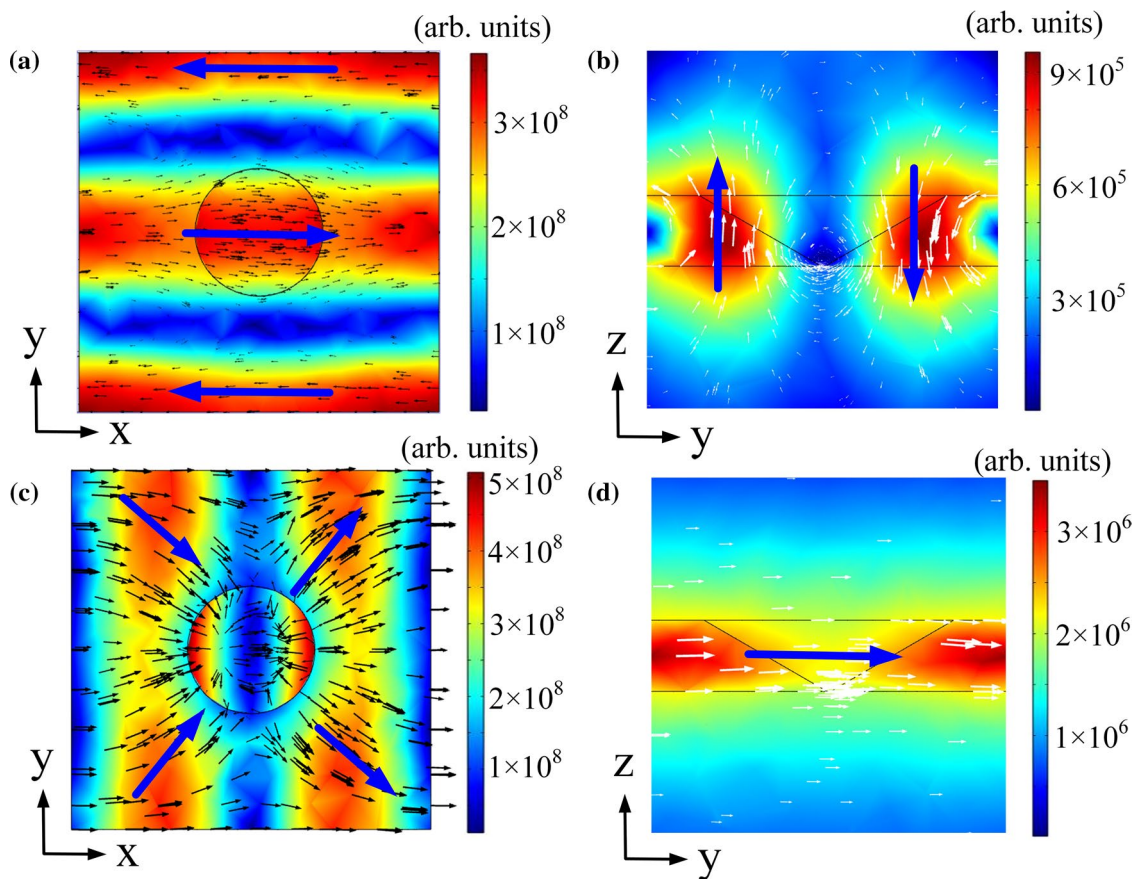**Fig. 3** (a) Scattering power of multipole decomposition; (b) effective impedance of the metasurface.

Fig. 4 (a), (c) Electric field and (b), (d) magnetic field of the conical hole at (a), (b) 1.255 μm and (c), (d) 1.087 μm, respectively. The black arrows are the current vector, the white arrows are the magnetic field vector, and the blue arrow indicates the direction (Color figure online).

white arrow in Fig. 4b represents the magnetic field vector, while the blue arrow represents the direction. The left upward magnetic field and the right downward magnetic field form the TD, which is also the main resonance mode of 1.255 μm. Figure 4c shows the electric field at 1.087 μm has four directions, which can form an EQ. In Fig. 4d, the magnetic field propagates only along the y-axis. Therefore, an MD is formed. Analyzing the electric and magnetic fields at 1.087 μm shows that EQ and MD are formed, which correspond to the multipole decomposition results in Fig. 3a.

In addition to considering the resonance mode, attention should also be paid to the location and the size of the electric field enhancement area. Figure 5a and b shows the cross-section of the electric field of the resonance of 1.255 μm at $Y = 0$ μm and $X = 0$ μm, respectively. As shown in Fig. 5c and d, the cross-section is the electric field of the resonance of the 1.087 μm at $Y = 0$ μm and $X = 0$ μm, respectively. The electric fields of 1.255 μm and 1.087 μm show significant enhancement. However, the location of these two resonance enhancements is different. The resonance electric fields of 1.255 μm and 1.087 μm are mainly located inside and outside of the conical hole, respectively. Meanwhile, the

difference in the size of the electric field enhancement area is not significant.

Previous studies have confirmed that the thickness of the analyte layer has a significant impact on frequency shift. Firstly, the frequency shift will increase as the thickness of the analyte layer increases. When the thickness of the analyte layer increases to a threshold, no matter how the thickness of the analyte layer increases, the frequency shift will not increase significantly.[39] The main reason for this phenomenon is that the electric field intensity decays exponentially in the vertical direction of the sample, resulting in a weak interaction between the electric field and the analyte. Therefore, when the analyte increases to a certain thickness, the frequency shift of the resonance peak will not change significantly.

According to the results shown in Fig. 5, the electric field is still enhanced at 0.5 μm from the surface of the structure. Therefore, we first investigated the variation in transmission with different thicknesses of analytes. As shown in Fig. 6a, the analyte has a refractive index of 1.5, and its transmission spectrum varies with its thickness. As the thickness of the analyte increases, the resonance peak of the two white
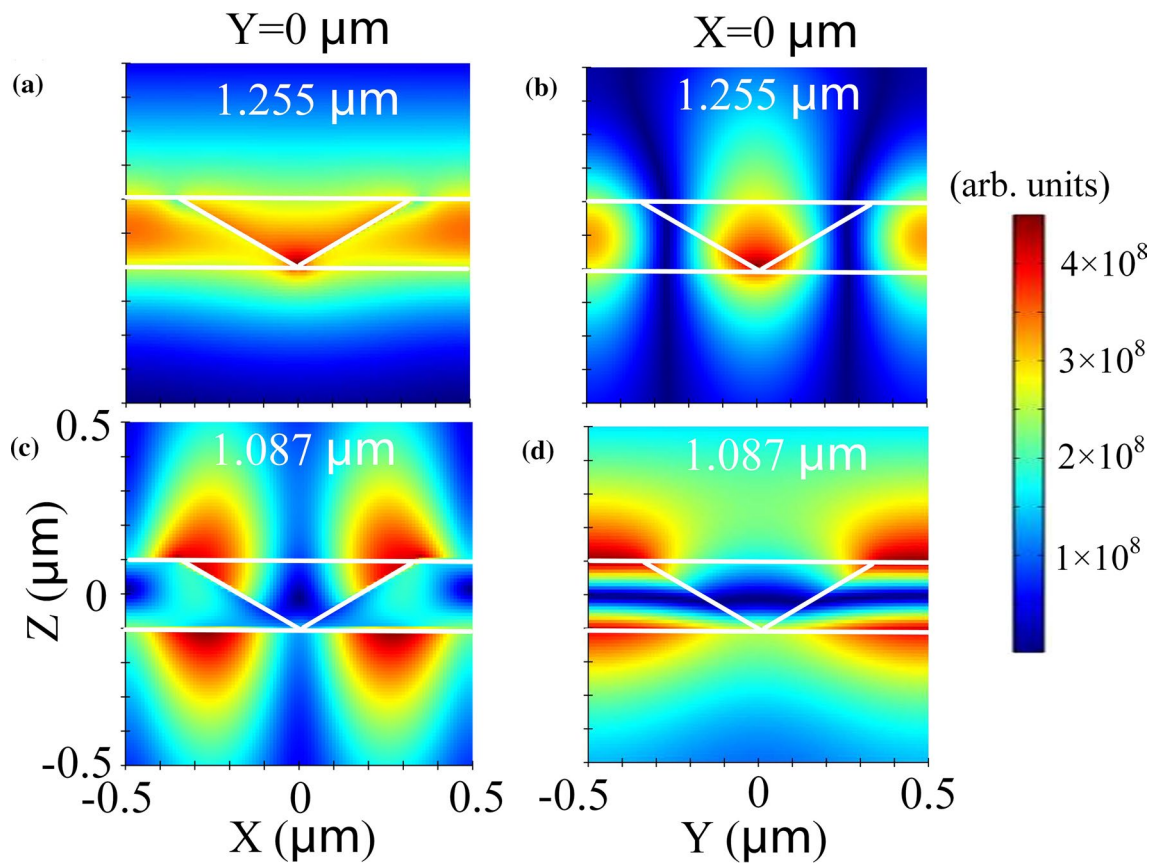
Fig. 5 Electric field of the conical hole at (a), (b) 1.255 μm and (c), (d) 1.087 μm, respectively.

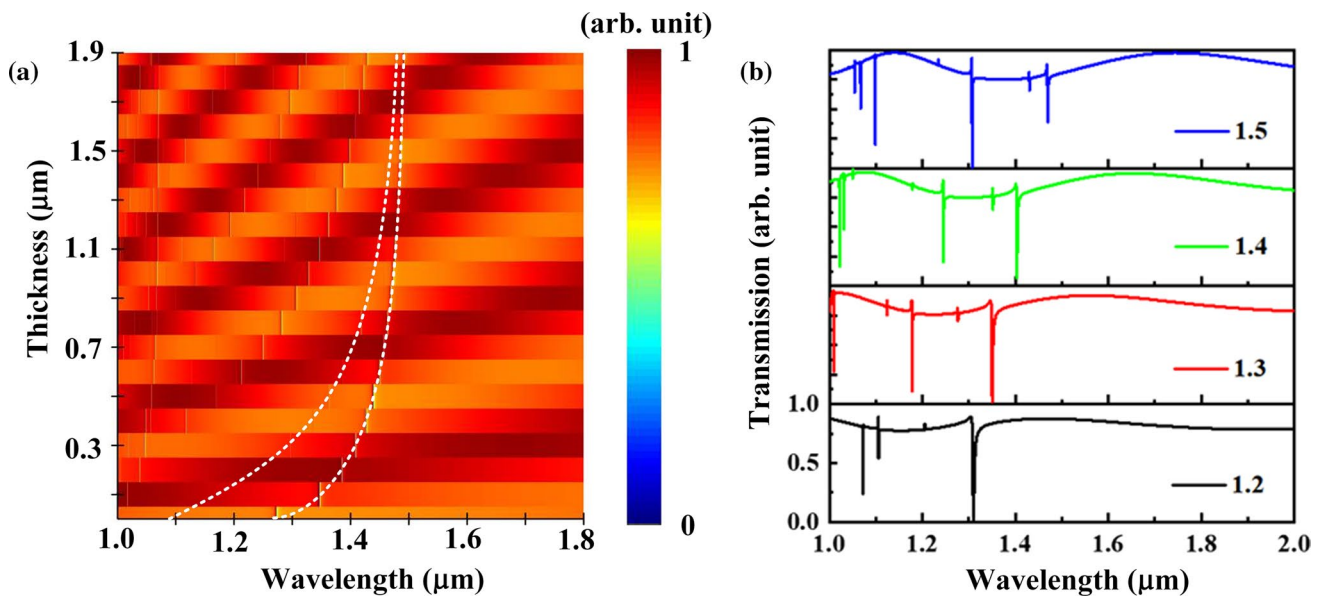**Fig. 6** (a) Transmission with varying analyte thickness; (b) transmission at 1-μm-thick analyte with analytes of different refractive indexes. The white dotted line in (a) shows the trend of the resonance with increasing analyte thickness.

dotted lines does not continue to increase at a thickness of about 1 μm. Therefore, the thickness of the analyte is chosen to be 1 μm, and the transmission obtained by varying the refractive index of the analyte is shown in Fig. 6b. As the refractive index of the analyte increases, the resonance peak exhibits a significant redshift. After calculation, the sensitivity of the resonance at 1.255 μm can reach 540 nm/RIU with a FOM (the ratio of the sensitivity to the full width of the half-peak) of 154.3, and sensitivity of the resonance at 1.087 μm can reach 749.6 nm/RIU. However, the resonance at 1.087 μm shows a significant decrease in intensity as the refractive index changes, which is not conducive to the detection of the signal. Therefore, resonance of 1.255 μm was chosen here for refractive index sensing.

In addition, compared to the previous all-dielectric toroidal dipole resonance structure reported in Table I, the sensitivity and FOM obtained here are significantly increased. Although some studies have higher FOM values, the sensitivity is lower. The high FOM is because they can produce a very narrow line width and obtain a high Q factor. And the low sensitivity is mainly because the local electric field enhancement is small, or the electric field enhancement is located inside of the structure, resulting in a weak interaction between the electric field and the analyte. Our structure can achieve higher sensitivity because the electric field enhancement has a large area, and the electric field enhancement is mainly outside the structure, so it can fully enhance the interaction between the electric field and the analyte.

Considering the real fabrication tolerance, the conical hole is more difficult to fabricate in practice, and an ellipsoidal hole may be obtained in the end. Therefore, the conical hole is changed to an ellipsoid hole. The long axis $L1$ is 0.7 μm, and half of the short axis $L2$ is 0.2 μm, as shown in Fig. 7a. When the conical hole is changed to an elliptical hole, the transmission is obtained in Fig. 7b, and the Q factor of resonance at 1.222 μm is 54. Compared to the electric field of the conical hole in Fig. 5, the electric field of the ellipsoidal hole structure shown in Fig. 7c and d is weak, which leads to a low Q factor. However, there is an increase in the area of the electric field enhancement.

Next, we investigated the effect of the ellipsoidal hole on refractive index sensing. When the ellipsoidal hole covers the analyte with a thickness of 1 μm, the sensitivity of the TD obtained from the simulation in Fig. 8a can reach 590 nm/RIU and FOM of 62.6. Although structural changes lead to low Q factors, the increase in the area of the electric field enhances the light–matter interaction. Therefore, it can be found that the fabrication tolerance has very little effect on the refractive index sensing, which indicates that the structure has a certain robustness. This is of great significance for the practical application of the structure. In addition, when the height H of the conical hole is fixed, the resonance is redshifted, and the line width of the resonance peak is also narrowed as the thickness of the structure increases, as shown in Fig. 8b. Multiple resonance peaks also appear as the thickness of the structure increases. Multiple resonance peaks can appear in more abundant electromagnetic resonance modes, so the sensitivity detection of multiple resonance peaks can be realized based on the different thicknesses of the structure and multiple wavelengths, which can be further optimized to improve the refractive index sensitivity and FOM.

Conclusion

The all-dielectric conical hole structure obtains toroidal dipole resonance, which leads to significant enhancement of light–matter interaction and large-area electric field. Moreover, the refractive index sensitivity and FOM can reach 540 nm/RIU and 154.3, respectively. Compared to the previous all-dielectric toroidal dipole resonance metasurfaces, the conical hole structure indicates a substantial improvement in sensing performance. The modification of the conical hole into an elliptical hole retains high sensitivity, confirming that the structure has a certain robustness, which is of great significance for practical application. At the same time, by changing the thickness of the structure, multiple resonances can be realized, and thus high-sensitivity

Table I Performance index parameters of refractive index sensing based on a toroidal dipole all-dielectric metasurface

| Structure	Material	Sensitivity	FOM	Year
Rectangular microporous structure	Silicon and quartz (loss)	161 nm/RIU	~	2020[40]
Asymmetric two parallel block structure	Titanium oxide and quartz (lossless)	80.6 nm /RIU	80.6 RIU^{-1}	2020[41]
Two semicircles	Silicon and quartz (lossless)	70 nm /RIU	2970 RIU^{-1}	2022[42]
Asymmetric X-type block structure	Silicon and quartz (lossless)	321 nm/RIU	5262 RIU^{-1}	2023[43]
Conical hole structure	Glass (LaSF) (lossless)	540 nm/RIU	154.3 RIU^{-1}	This work
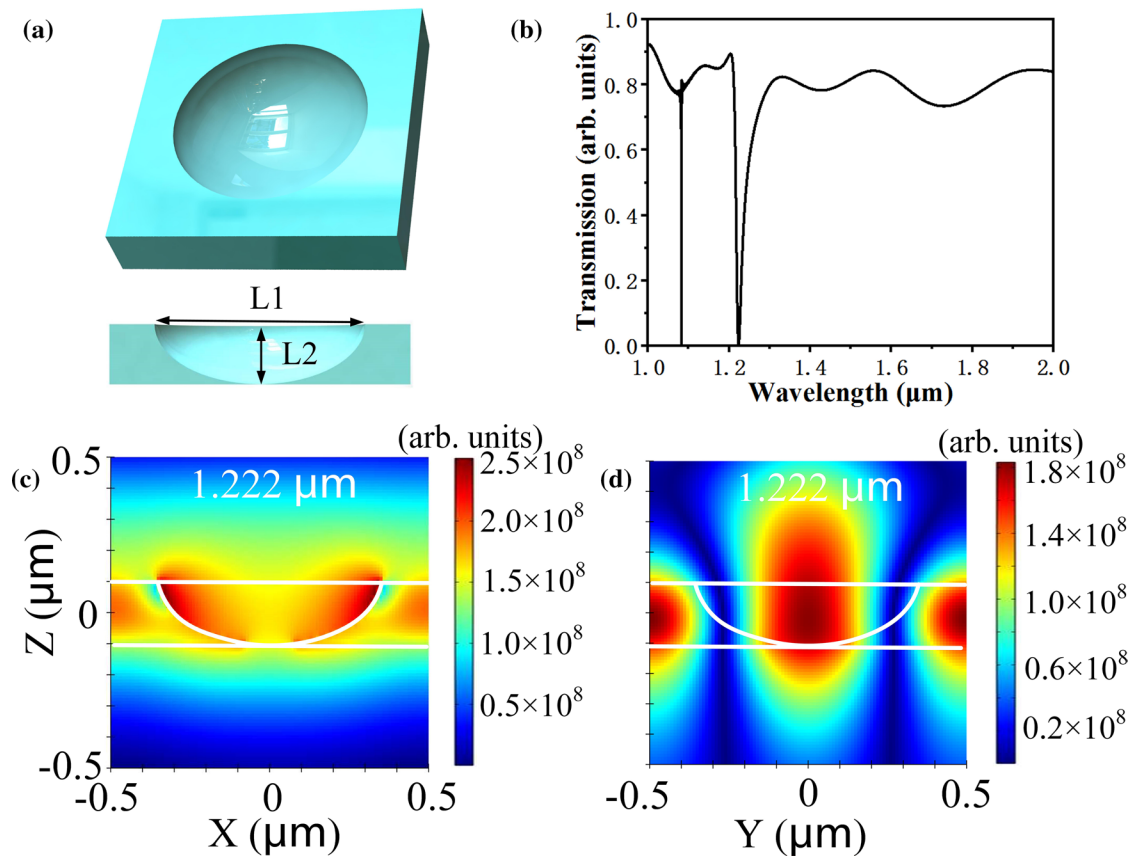
Fig. 7 (a) The three-dimensional image and cross-section of the ellipsoidal hole; (b) transmission of the ellipsoidal hole; electric field of the ellipsoidal hole in the (c) *XZ* and (d) *YZ* planes.
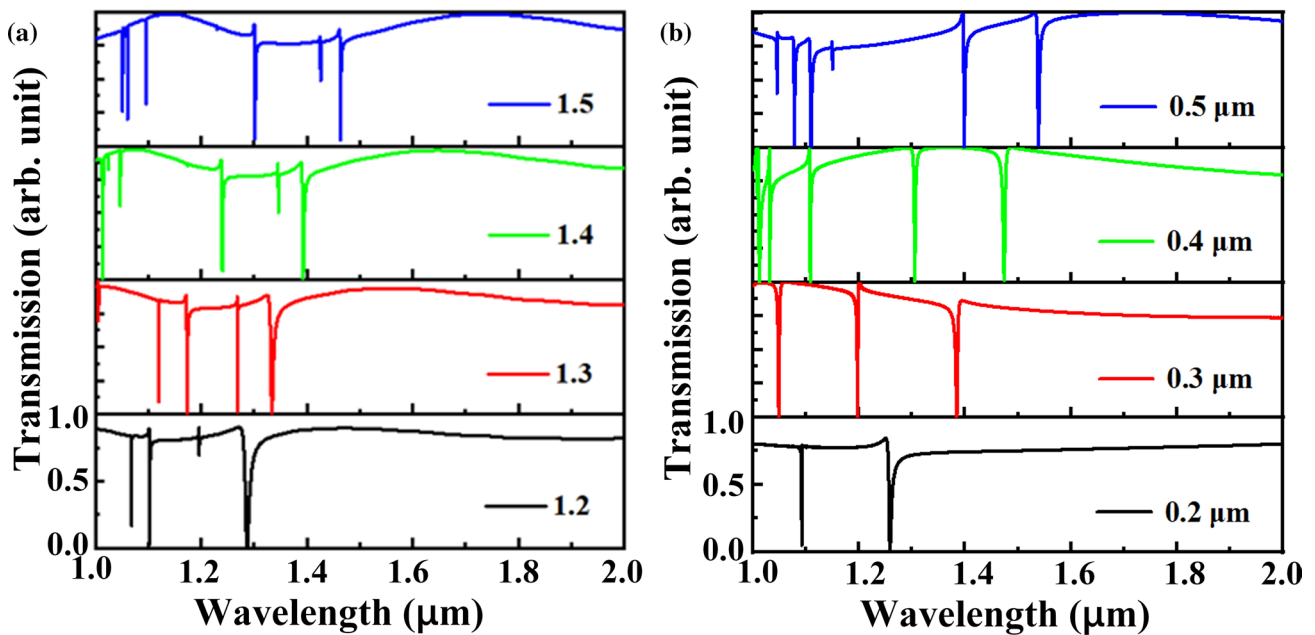

Fig. 8 (a) Transmission of an ellipsoidal hole structure at 1-µm-thick analyte with analytes of different refractive indexes; (b) transmission of conical hole structure varying with increasing thickness of the structure.

detection at multiple wavelengths can also be achieved based on multiple resonance modes.

Data Availability The datasets are available from the corresponding author on reasonable request.

Conflict of interest The authors declare no conflict of interest.

References

1. Y.Y. Chen, J.C. Liu, Z.C. Yang, J.S. Wilkinson, and X.H. Zhou, Optical biosensors based on refractometric sensing schemes: a review. *Biosens. Bioelectron.* 144, 111693 (2019)
2. G. Zanchetta, R. Lanfranco, F. Giavazzi, T. Bellini, and M. Buscaglia, Emerging applications of label-free optical biosensors. *Nanophotonics* 6(4), 627 (2017)
3. J.J. Ong, T.D. Pollard, A. Goyanes, S. Gaisford, M. Elbadawi, and A.W. Basit, Optical biosensors-Illuminating the path to personalized drug dosing. *Biosens. Bioelectron.* 188, 113331 (2021)
4. H. Li, S. Yu, L. Yang, and T.G. Zhao, High Q-factor multi-Fano resonances in all-dielectric double square hollow metamaterials. *Opt. Laser Technol.* 140, 107072 (2021)
5. V.R. Tuz, V.V. Khardikov, A.S. Kupriianov, K.L. Domina, S. Xu, H. Wang, and H.B. Sun, High-quality trapped modes in all-dielectric metamaterials. *Opt. Express* 26(3), 2905 (2018)
6. J.F. Algorri, D.C. Zografopoulos, A. Ferraro, B. García-Cámara, R. Beccherelli, and J.M. Sánchez-Pena, Ultrahigh-quality factor resonant dielectric metasurfaces based on hollow nanocuboids. *Opt. Express* 27(5), 6320 (2019)
7. P.C. Wu, C.Y. Liao, V. Savinov, T.L. Chung, W.T. Chen, Y.W. Huang, P.R. Wu, Y.H. Chen, A.Q. Liu, N.I. Zheludev, and D.P. Tsai, Optical anapole metamaterial. *ACS Nano* 12(2), 1920 (2018)
8. J. Valentine, S. Zhang, T. Zentgraf, E. Ulin-Avila, D.A. Genov, G. Bartal, and X. Zhang, Three-dimensional optical metamaterial with a negative refractive index. *Nature* 455(7211), 376 (2008)
9. P. Moitra, Y.M. Yang, Z. Anderson, I.I. Kravchenko, D.P. Briggs, and J. Valentine, Realization of an all-dielectric zero-index optical metamaterial. *Nat. Photonics* 7(10), 791 (2013)
10. D. Rocco, V.F. Gili, L. Ghirardini, L. Carletti, I. Favero, A. Locatelli, G. Marino, D.N. Neshev, M. Celebrano, M. Finazzi, G. Leo, and C.D. Angelis, Tuning the second-harmonic generation in AlGaAs nanodimers via non-radiative state optimization. *Photonics Res.* 6(5), 6 (2018)
11. V.F. Gili, L. Ghirardini, D. Rocco, G. Marino, I. Favero, I. Roland, G. Pellegrini, L. Duò, M. Finazzi, L. Carletti, A. Locatelli, A. Lemaître, D. Neshev, C.D. Angelis, G. Leo, and M. Celebrano, Metal–dielectric hybrid nanoantennas for efficient frequency conversion at the anapole mode. *Beilstein J. Nanotechnol.* 9, 2306 (2018)
12. J. Yao, J.Y. Ou, V. Savinov, M.K. Chen, H.Y. Kuo, N.I. Zheludev, and D.P. Tsai, Plasmonic anapole metamaterial for refractive index sensing. *PhotoniX* 3, 23 (2022)
13. L. Liang, X. Hu, L. Wen, Y.H. Zhu, X.G. Yang, J. Zhou, Y.X. Zhang, I.E. Carranza, J. Grant, C.P. Jiang, D.R.S. Cumming, B.J. Li, and Q. Chen, Unity integration of grating slot waveguide and microfluid for terahertz sensing. *Laser Photonics Rev.* 12(11), 1800078 (2018)
14. M. Beruete and I. Jáuregui-López, Terahertz sensing based on metasurfaces. *Adv. Opt. Mater.* 8(3), 1900721 (2020)
15. Y.B. Zhang, W.W. Liu, Z.C. Li, Z. Li, H. Cheng, S.Q. Chen, and J.G. Tian, High-quality-factor multiple fano resonances for refractive index sensing. *Opt. Lett.* 43(8), 1842 (2018)
16. R. Yahiaoui, A.C. Strikwerda, and P.U. Jepsen, Terahertz plasmonic structure with enhanced sensing capabilities. *IEEE Sens. J.* 16(8), 2484 (2016)
17. S. Mobasser, S. Poorgholam-Khanjari, M. Bazgir, and F.B. Zarrabi, Highly sensitive reconfigurable plasmonic metasurface with dual-band response for optical sensing and switching in the mid-infrared spectrum. *J. Electron. Mater.* 50, 120 (2021)
18. L.H. Guo, Z.X. Zhang, Q. Xie, W.X. Li, F. Xia, M. Wang, H. Feng, C.L. You, and M.J. Yun, Toroidal dipole bound states in the continuum in all-dielectric metasurface for high-performance refractive index and temperature sensing. *Appl. Surf. Sci.* 156408, 0169 (2023)
19. V.A. Popescu, A.K. Sharma, and Y.K. Prajapati, Graphene-based plasmonic detection of magnetic field and gaseous medium with photonic spin hall effect in a broad terahertz region. *J. Electron. Mater.* 51, 2889 (2022)
20. M. Karthikeyan, P. Jayabala, S. Ramachandran, S.S. Dhanabalan, T. Sivanesan, and M. Ponnusamy, Tunable optimal dual band metamaterial absorber for high sensitivity THz refractive index sensing. *Nanomaterials* 12(15), 2693 (2022)
21. A. Tognazzi, D. Rocco, M. Gandolfi, A. Locatelli, L. Carletti, and C.D. Angelis, High quality factor silicon membrane metasurface for intensity-based refractive index sensing. *Optics* 2(3), 193 (2021)
22. V.G. Kravets, A.V. Kabashin, W.L. Barnes, and A.N. Grigorenko, Plasmonic surface lattice resonances: a review of properties and applications. *Chem. Rev.* 118(12), 5912 (2018)
23. Y. Liang, Q.L. Tan, W. Zhou, X. Zhou, Z.A. Wang, G.Y. Zhou, and X.G. Huang, Refractive index sensing utilizing tunable polarization conversion efficiency with dielectric metasurface. *J. Lightwave Technol.* 39(2), 682 (2021)
24. M.F. Limonov, M.V. Rybin, A.N. Poddubny, and Y.S. Kivshar, Fano resonances in photonics. *Nat. Photonics* 11(9), 543 (2017)
25. X. Chen, W.H. Fan, X.Q. Jiang, and H. Yan, High-Q toroidal dipole metasurfaces driven by bound states in the continuum for ultrasensitive terahertz sensing. *J. Lightwave Technol.* 40(7), 2181 (2022)
26. X. Chen, W.H. Fan, and H. Yan, Toroidal dipole bound states in the continuum metasurfaces for terahertz nanofilm sensing. *Opt. Express* 28(11), 17102 (2020)
27. R.D. Wang, L. Xu, J.Y. Wang, L. Sun, Y.N. Jiao, Y. Meng, S. Chen, C. Chang, and C.H. Fan, Electric fano resonance-based terahertz metasensors. *Nanoscale* 13(44), 18467 (2021)
28. K. Koshelev, S. Lepeshov, M.K. Liu, A. Bogdanov, and Y. Kivshar, Asymmetric metasurfaces with high-Q resonances governed by bound states in the continuum. *Phys. Rev. Lett.* 121(19), 193903 (2018)
29. X.G. Zhao, C.X. Chen, K. Kaj, I. Hammock, Y.W. Huang, R.D. Averitt, and X. Zhang, Terahertz investigation of bound states in the continuum of metallic metasurfaces. *Optica* 7(11), 1548 (2020)
30. A. Kodigala, T. Lepetit, Q. Gu, B. Bahari, Y. Fainman, and B. Kanté, Lasing action from photonic bound states in continuum. *Nature* 541(7636), 196 (2017)
31. B.W. Liu, Y. Peng, Z.M. Jin, X. Wu, H.Y. Gu, D.S. Wei, Y.M. Zhu, and S.L. Zhuang, Terahertz ultrasensitive biosensor based on wide-area and intense light-matter interaction supported by QBIC. *Chem. Eng. J.* 462, 142347 (2023)
32. H.H. Hsiao, Y.C. Hsu, A.Y. Liu, J.C. Hsieh, and Y.H. Lin, Ultrasensitive refractive index sensing based on the quasi-bound states

in the continuum of all-dielectric metasurfaces. *Adv. Opt. Mater.* 10, 2200812 (2022)

33. W.J. Chen, M. Li, W.H. Zhang, and Y.H. Chen, Dual-resonance sensing for environmental refractive index based on quasi-BIC states in all-dielectric metasurface. *Nanophotonics* 12(6), 11477 (2023)

34. V. Savinov, V.A. Fedotov, and N.I. Zheludev, Toroidal dipolar excitation and macroscopic electromagnetic properties of metamaterials. *Phys. Rev. B* 89(20), 205112 (2014)

35. A.A. Basharin, M. Kafesaki, E.N. Economou, C.M. Soukoulis, V.A. Fedotov, V. Savinov, and N.I. Zheludev, Dielectric metamaterials with toroidal dipolar response. *Phys. Rev. X* 5(1), 011036 (2015)

36. G. Feng, Z.H. Chen, X.W. Wang, X. Liu, F. Sun, and Y.B. Yang, Ultra-broadband terahertz absorber based on double truncated pyramid structure. *Mater. Today Commun.* 31, 103624 (2022)

37. X.W. Zhang, W. Pan, T. Shen, and Y. Li, Research on terahertz band demultiplexer based on metamaterials. *Infrared Techn.* 43(6), 532 (2021)

38. A. Ahmadivand, B. Gerislioglu, R. Ahuja, and Y.K. Mishra, Terahertz plasmonics: the rise of toroidal metadevices towards immunobiosensings. *Mater. Today* 32, 108 (2020)

39. K. Shih, P. Pitchappa, L. Jin, C.H. Chen, R. Singh, and C.K. Lee, Nanofluidic terahertz metasensor for sensing in aqueous environment. *Appl. Phys. Lett.* 113, 071105 (2018)

40. J. Jeong, M.D. Goldflam, S. Campione, J.L. Briscoe, P.P. Vabishchevich, J. Nogan, M.B. Sinclair, T.S. Luk, and I. Brener, High

quality factor toroidal resonances in dielectric metasurfaces. *ACS Photonics* 7(7), 1699 (2020)

41. Y. Chen, C. Zhao, Y.Z. Zhang, and C.W. Qiu, Integrated molar chiral sensing based on high-Q metasurface. *Nano Lett.* 20(12), 8696 (2020)

42. L.X. Yuan, C.Q. Qiu, Z. Liao, M.H. Gong, Y. Long, R. Yang, and Z.R. Zhang, Nanoscale refractive index sensor with ultrahigh figure of merit based on toroidal dielectric metasurfaces. *Opt. Commun.* 528, 128988 (2023)

43. S.J. Tu, X.X. Liu, K.L. Liang, Q. Fu, Y.L. Wang, Q.G. Du, and Z.Y. Li, An ultra-high figure of merit refractive index sensor with Mie lattice resonance of a toroidal dipole in an all-dielectric metasurface array in the near-infrared. *J. Phys. D Appl. Phys.* 56(11), 115101 (2023)